

Article

Adaptive Marginal Costs-Based Distributed Economic Control of Microgrid Clusters Considering Line Loss

Xiaoqian Zhou, Qian Ai * and Hao Wang

School of Electronic Information and Electrical Engineering, Shanghai Jiao Tong University, Dongchuan Road, Shanghai 200240, China; xqzhou@sjtu.edu.cn (X.Z.); Joshua_H@sjtu.edu.cn (H.W.)

* Correspondence: aiqian@sjtu.edu.cn; Tel.: +86-21-3429-4584

Received: 23 November 2017; Accepted: 1 December 2017; Published: 6 December 2017

Abstract: When several microgrids (MG) are interconnected into microgrid clusters (MGC), they have great potential to improve their reliability. Traditional droop control tends to make the total operating costs higher as the power is distributed by capacity ratios of distributed energy resources (DERs). This paper proposes an adaptive distributed economic control for islanded microgrids which considers line loss, specifically, an interesting marginal costs-based economic droop control is proposed, and consensus-based adaptive controller is applied, to deal with power limits and capacity constraints for storage. The whole expense can be effectively lowered by achieving identical marginal costs for DERs in MGC. Specially, the capacity constraints only for storages are also included to do further optimization. Moreover, consensus-based distributed secondary controllers are used to rapidly restore system frequency and voltage magnitudes. The above controllers only need to interact with neighbor DERs by a sparse communication network, eliminating the necessity of a central controller and enhancing the stability. A MGC, incorporating three microgrids, is used to verify the effectiveness of the proposed methods.

Keywords: microgrid clusters; marginal costs; line loss; consensus algorithm; distributed economic control; distributed secondary controllers

1. Introduction

Microgrids can be considered autonomous small-type power distribution systems, which are integrated with several types of distributed energy resources (DERs) and loads [1]. For microgrids incorporating photovoltaic and wind power generation, storage and a conventional power grid [2], presents a mathematical model of a DC microgrid, and this model is utilized to propose, implement and analyze a new system of voltage management in this microgrid. In [3], for microgrids including the increased penetration of renewable energy sources, storage batteries, DERs and loads, a robust energy management solution to facilitate the optimum and economic control of energy flows throughout a microgrid network, was proposed. Due to the differences in infrastructure and natural conditions, each microgrid contains distinct DERs and loads; it is beneficial to enhance the reliability and lower the expense if several microgrids are interconnected into microgrid clusters (MGC) for operation [4]. At present, the research on MGC is still at the initial stage—in [5], a hierarchical control structure including primary, secondary, and tertiary levels was proposed, to handle power sharing among a cluster of DC microgrids. A consensus-based, distributed control strategies for voltage regulation and power flow control of DC microgrid clusters was presented in [6] and an SOC-based adaptive droop method was introduced at the primary level to equalize SOC of batteries inside each microgrid (MG). Decentralized control of two DC microgrids interconnected with a tie-line was examined in [7], and a decentralized control approach was proposed to control each MG and bus voltage fluctuation in an allowable range. A real-time tertiary control algorithm for DC microgrids was developed

and implemented in [8], and to overcome renewable energy intermittency, the developed algorithm virtually aggregated neighboring microgrids into clusters. Aimed at microgrid clusters, including AC and DC sub-microgrids, an autonomous coordination control strategy was applied in [9]. However, the above references [5–9] put an emphasis on DC microgrids, and did not take operating costs into consideration, so these methods lack economy. Aimed at AC microgrid clusters, traditional droop control is often applied in autonomous microgrids; however, this control distributes power by the capacity ratio [10], so it is easy to make the total operational costs higher as the generation costs and operating characteristics of different types of DERs are varied. The centralized optimization is effective for improving economy, as it will take advantage of information from all DERs, and computes the optimal result in the central system, then sends the regulating commands to the DERs. Although the accuracy is high, it is vulnerable to central point of failures and communication failures, so its reliability is low.

In recent years, distributed economic operation of microgrids has attracted researchers' attention. For distributed economic dispatch, an extended distributed model predictive control framework has been applied to a smart grid case study. Specifically, a combined environmental and economic dispatch problem was formulated and solved in [11]. In [12], the framework of real-time collaborative dispatch was proposed by using the multi-agent consensus theory to solve a real-time dispatch problem in the islanded multi-microgrid. The problem of electrical energy transaction between islanded MGs was optimized by making use of a sub-gradient cost minimization algorithm, in [13,14]. A projected gradient and finite-time averaged consensus algorithm was used to deal with an economic dispatch problem, including thermal generators and wind turbines, in [15]. For distributed control, most references are aimed at distributed secondary control [16–19]; few papers put an emphasis on economic control. A kind of economic nonlinear droop controller was designed in [20–22] to make expensive DERs generate less power, and more power is produced by cheaper DERs. The proposed controller can effectively lower the operating expense; however, it is designed on the basis of DER generation costs, instead of marginal costs, thereby it cannot realize the optimal operation of DERs. Moreover, secondary frequency and voltage regulation are not considered in these papers. By considering the optimal economic operation, Chen Su [23] proposed a kind of marginal costs-voltage droop control, however equal marginal costs are not realized in primary control because of heterogeneous line impedance, which means secondary control must be used to finish this function—this makes the system become complicated. In addition, renewable energy and storage devices are not considered in this paper. To achieve identical marginal costs among DERs, a kind of autonomous three-level controller was presented in [24]; however, its dynamic response was slower, due to the adoption of a lower-pass filter that was used to reduce the effect of non-linear droop control on the system stability. In [25], which was aimed at the traditional droop-controlled microgrids, a consensus algorithm was designed to realize the economic operation based on equal incremental rate; however, the system stability was weaker because the dominant mode had to be used to control the direction of the increasing or decreasing marginal costs.

For AC microgrid clusters, considering economy requirements, this paper makes a contribution in the following areas; (i) an adaptive economic droop control framework, considering line loss among sub-microgrids is proposed; (ii) Apart from traditional power constraints of DERs, the capacity limits of storage units are also considered, i.e., if the storage has increased to 80% or decreased to 20% of its capacity, its adaptive controller is applied to draw the power of the storage to zero. (iii) to effectively restore the system frequency, a distributed secondary frequency controller (DSFC) is proposed to complete this goal in a distributed way and (iv) the whole design effectively lowers the operating costs of MGC.

Apart from the above original contributions, virtual impedance is used in a low-voltage network, where line impedance is mainly determined by resistive, to ensure that the output impedance is desirable at the line frequency [26,27] and a distributed secondary voltage controller (DSVC) from [10]

is used to reach a compromise between reactive power averaging and voltage regulation, by choosing proper weight coefficients.

The paper is organized as follows: Section 2 specifically introduces the problem of economic control in MGC, and the marginal costs of different types of DERs, which are modeled based on their power characteristics, are all listed by the condition of line loss (with vs. without) among sub-microgrids. Adaptive economic droop control is proposed in Section 3; specifically, marginal costs-frequency droop control is applied, and consensus-based adaptive controller is also given at length here. DSFC and DSVC are both presented in Section 4. In Section 5, The implementation process of the overall distributed economic control, including the communication network topology of MGC and the overall control architecture, is clearly described. The proposed controllers are tested in Section 6 under a range of conditions. Section 7 gives a conclusion for this paper.

2. The Problem of Economic Control

On the basis of stable operation of MGC, economic control is mainly aimed at considering the economic factors to real-time control the relevant parameters, to achieve the lowest operating costs. In this paper, we do not consider the generation costs from reactive power, and only consider those from active power.

The generation costs from active power can be all written as a quadratic function, regardless of different types of DERs [20]. Here, we consider three kinds of DERs, respectively, conventional generators, renewable generators and storage devices.

For conventional generators, the generation costs can be expressed as a convex quadratic function, as shown in Equation (1):

$$\begin{aligned} i = 1, 2, \dots, N_G, 0 \leq P_i \leq P_{i,\max} \\ C_{i,G}(P_i) = a_i P_i^2 + b_i P_i + c_i, \end{aligned} \quad (1)$$

where P_i is the active power of the generator i , $P_{i,\max}$ is the power maximum of the generator i , a_i, b_i, c_i are positive cost coefficients of conventional generators. $C_{i,G}(P_i)$ is the generation cost of generator i . N_G is the number of conventional generators.

To promote the effective use of renewable energy, we adopt a pseudo generation cost in this paper. According to [28], the generation costs of solar power or wind power can be formulated as:

$$\begin{aligned} j = 1, 2, \dots, N_R, 0 \leq P_j \leq P_{j,\max} \\ C_{j,R}(P_j) = \frac{(P_j - P_{j,\max})^2}{P_{j,\max}} = \frac{1}{P_{j,\max}} P_j^2 - 2P_j + P_{j,\max} = a_j P_j^2 + b_j P_j + c_j \end{aligned} \quad (2)$$

where $P_{j,\max}$ is the predicted power capacity that can be obtained from maximum power prediction technology, $C_{j,R}(P_j)$ is a convex quadratic cost function for a renewable generator j . N_R is the number of renewable generators. Compared with Equation (1), we can consider $a_j = 1/P_{j,\max}$, $b_j = -2$, $c_j = P_{j,\max}$, so the same expression of cost function can be achieved between conventional generators and renewable generators. Moreover, the generation cost tends to zero as the power increases to $P_{j,\max}$. This means that when the generation cost arrives at the minimum, the lowest renewable energy curtailment can be simultaneously obtained.

The generation cost function of battery k can be formulated as:

$$\begin{aligned} k = 1, 2, \dots, N_S, -P_{k,\max} \leq P_k \leq P_{k,\max} \\ C_{k,S}(P_k) = a_k P_k^2 + c_k \end{aligned} \quad (3)$$

where $C_{k,S}(P_k)$ is a continuous convex quadratic function for battery k ; a_k, c_k are non-negative cost parameters; and N_S is the number of battery. P_k is the charging or discharging power that represents discharging to the load if P_k is positive, on the contrary, battery k is charged from other DERs if P_k is negative. $P_{k,\max}$ is the largest discharging power of battery k .

2.1. Marginal Costs without Considering Line Loss

When line loss is not considered, the marginal cost of a DER is the derivative of the corresponding generation cost, as shown in Equations (1)–(3)—we can call it traditional marginal costs (TMC) in this paper. According to equal incremental rate criteria [25], the whole operating expenses of microgrids can be the minimum if TMC from DERs are all the same.

The marginal cost of conventional generator i and renewable generator j can be respectively described as:

$$\begin{aligned} L_{i,G}(P_i) &= \frac{dC_{i,G}(P_i)}{dP_i} = 2a_i P_i + b_i > 0 \\ L_{j,R}(P_j) &= \frac{dC_{j,R}(P_j)}{dP_j} = 2a_j P_j + b_j = 2 \frac{P_j}{P_{j,\max}} - 2 \leq 0 \end{aligned} \quad (4)$$

That is,

$$L_{i,G}(P_i) > L_{j,R}(P_j) \quad (5)$$

From Equation (5), it can be clearly seen that the marginal costs of conventional generators are always greater than those of renewable generators. This means that renewable generators always have a priority to generate power for achieving effective use of renewable energy.

The marginal cost of battery k is also a continuous function because the gradient of cost function at $P_k = 0$ is 0, as listed in Equation (6); this guarantees the availability of equal increment rate criteria. In this paper, \bar{a}_k , \underline{a}_k is, respectively, the cost coefficient for discharging/charging, and \bar{a}_k is much larger than \underline{a}_k .

$$L_{k,S}(P_k) = \frac{dC_{k,S}(P_k)}{dP_k} = \begin{cases} 2\bar{a}_k P_k + b_k = 2\bar{a}_k P_k + 0 \geq 0 & P_k \geq 0 \\ 2\underline{a}_k P_k + b_k = 2\underline{a}_k P_k + 0 < 0 & P_k < 0 \end{cases} \quad (6)$$

From Equations (4)–(6), according to equal increment rate criteria, two scenarios should also be considered, as follows:

- In the light load scenario, conventional generators do not generate any power—the power can be distributed among renewable generators and storage devices. According to equal increment rate criteria, storage k will be charged to achieve marginal costs, similar to that of renewable generators, and this is feasible in practical operating conditions.
- By contrast, in the heavy load scenario, the power of renewable generators reach their upper limits and the rest of the power can be distributed by conventional generators and storage devices, i.e., storage k will discharge in this case.

Moreover, in the light load scenario where equal marginal costs are realized among renewable generators, the active power of arbitrary renewable generators, m and n , are also proportional to their predicted power capacity, as follows:

$$\frac{P_m}{P_{m,\max}} = \frac{P_n}{P_{n,\max}} \quad (7)$$

2.2. Marginal Costs with Considering Line Loss

When line loss among sub-microgrids is considered, marginal costs with line loss (LLMC) should be applied in the economic control of MGC. In this paper, only line loss among sub-microgrids is considered. In this condition, equality constraint Equation (8) should be considered on the basis of the objective function Equation (9).

$$\sum_{i=1}^{N_G} P_i + \sum_{j=1}^{N_R} P_j + \sum_{k=1}^{N_S} P_k - P_D - P_L = 0 \quad (8)$$

$$\min \left(\sum_{i=1}^{N_G} C_{i,G}(P_i) + \sum_{j=1}^{N_R} C_{j,R}(P_j) + \sum_{k=1}^{N_S} C_{k,S}(P_k) \right) \quad (9)$$

where P_D is the total active power load, and P_L is the sum of line loss. N_G , N_R , N_S are, respectively, the number of conventional generators, renewable generators and storage devices.

According to Equations (8) and (9), using Lagrange multiplier λ , Lagrange function can be given as:

$$J(P_i, P_j, P_k, \lambda) = \left(\sum_{i=1}^{N_G} C_{i,G}(P_i) + \sum_{j=1}^{N_R} C_{j,R}(P_j) + \sum_{k=1}^{N_S} C_{k,S}(P_k) \right) - \lambda \left(\sum_{i=1}^{N_G} P_i + \sum_{j=1}^{N_R} P_j + \sum_{k=1}^{N_S} P_k - P_D - P_L \right) \quad (10)$$

The LLMC ($SL_{i,G}(P_i)$, $SL_{j,R}(P_j)$, $SL_{k,S}(P_k)$) of conventional generators, renewable generators and storage devices is, respectively, the value of λ at the extremum of Lagrange function. Therefore, LLMC can be listed as:

$$\frac{\partial J(P_i, P_j, P_k, \lambda)}{\partial P_i} = \frac{\partial C_{i,G}(P_i)}{\partial P_i} - \lambda \left(1 - \frac{\partial P_L}{\partial P_i} \right) = 0$$

$$\downarrow$$

$$SL_{i,G}(P_i) = \lambda = \frac{\partial C_{i,G}(P_i)}{\partial P_i} \left[1 / \left(1 - \frac{\partial P_L}{\partial P_i} \right) \right] \quad (11)$$

Similarly, $SL_{j,R}(P_j)$, $SL_{k,S}(P_k)$ can also be solved as:

$$SL_{j,R}(P_j) = \frac{\partial C_{j,R}(P_j)}{\partial P_j} \left[1 / \left(1 - \frac{\partial P_L}{\partial P_j} \right) \right]$$

$$SL_{k,S}(P_k) = \frac{\partial C_{k,S}(P_k)}{\partial P_k} \left[1 / \left(1 - \frac{\partial P_L}{\partial P_k} \right) \right] \quad (12)$$

where $\partial P_L / \partial P_i$, $\partial P_L / \partial P_j$, $\partial P_L / \partial P_k$ is called the line loss correction factor (LLCF).

Let us compute LLCF, for the active power of the branch, i - j , in the AC electrical network under the condition of neglecting earth branch can be expressed as:

$$P_{ij} = U_i^2 g_{ij} - U_i U_j (g_{ij} \cos \theta_{ij} + b_{ij} \sin \theta_{ij}) \quad (13)$$

where, the voltage of node i , j is $\dot{U}_i = U_i e^{j\theta_i}$, $\dot{U}_j = U_j e^{j\theta_j}$. The conductance and susceptance of the branch i - j are, respectively, g_{ij} and b_{ij} ; resistance and reactance are separately, R_{ij} and X_{ij} . AC microgrids are low voltage networks and line resistance is mainly resistive, so $R_{ij} \geq X_{ij}$, $|g_{ij}| \geq |b_{ij}|$. Due to θ_{ij} being small, $\cos \theta_{ij} \approx 1$, $\sin \theta_{ij} \approx \theta_{ij} \approx 0$. Therefore, (13) can be simplified as:

$$P_{ij} = U_i^2 g_{ij} - U_i U_j g_{ij} \quad (14)$$

Therefore, the node injection power P_{Ini} is expressed as:

$$P_{Ini} = P_{Gi} - P_{Di} = \sum_{jNi} P_{ij} = \sum_{jNi} g_{ij} U_i (U_i - U_j) \quad (15)$$

where P_{Gi} is the electrical source of node i from conventional generators, renewable generators or storage devices; P_{Di} is the load of node i ; jNi shows that the node j must be directly connected with node i , but the condition $i = j$ is not included.

The sum of line loss is the sum of node injection power,

$$P_L = \sum_{i=1}^n P_{Ini} = \sum_{i=1}^n \sum_{jNi} g_{ij} U_i (U_i - U_j) \quad (16)$$

The LLCF of DER i can be computed from (15) and (16),

$$\frac{\partial P_L}{\partial P_{Gi}} = \frac{\partial P_L}{\partial U_i} \frac{\partial U_i}{\partial P_{Gi}} = \frac{\sum_{jNi} 2(U_i - U_j) g_{ij}}{\sum_{jNi} (2U_i - U_j) g_{ij}} \quad (17)$$

From Equations (11), (12) and (17), the LLMC of conventional generators, renewable generators and storage devices can be all obtained. In a MGC, the total cost is the least if the LLMC of all DERs are the same.

In this paper, there are two types of operation modes—autonomously and collectively—for sub-microgrid i . Due to the relatively small scale for sub-microgrids, line loss is not considered in autonomous mode. In contrast, line loss between sub-microgrids needs to be included in collective mode. The corresponding marginal costs in two modes are respectively listed in Equation (18).

$$L_i(P_i) = \begin{cases} L_{i,G}(P_i), L_{i,R}(P_i), L_{i,S}(P_i) & \text{TMC} \quad \textit{autonomously} \\ SL_{i,G}(P_i), SL_{i,R}(P_i), SL_{i,S}(P_i) & \text{LLMC} \quad \textit{collectively} \end{cases} \quad (18)$$

3. Adaptive Economic Droop Control

3.1. Marginal Costs-Frequency Droop Control

If power limits of DERs are not considered, minimal total operating costs can be achieved when marginal costs (Autonomously: TMC; Collectively: LLMC) for all DERs are equal. Therefore, in order to achieve economic operation of the MGC, on the basis of traditional P - f droop control ($f_i = f^* - m_i P_i$, m_i is the traditional droop coefficient), and considering the marginal cost of each DER, an $L_i(P_i) - f$ droop control is proposed, as follows:

$$f_i = f^* - \lambda_i L_i(P_i), \quad i = 1, 2, \dots, N_{\text{DER}} \quad (19)$$

where N_{DER} is the number of DERs, f^* is the nominal network frequency, P_i is the measured active power injection, f_i is the measured frequency of DER i . $L_i(P_i)$ is the TMC or LLMC of DER i , which has already been discussed in detail in Section 2 and λ_i is the economic droop coefficient. Equation (20) should be satisfied when choosing λ_i .

$$|\lambda_i| \leq \frac{\Delta f_{\text{max}}}{|L_i(P_i)|_{\text{max}}}, \quad \lambda_i \neq 0 \quad (20)$$

where Δf_{max} is the maximal frequency deviation.

3.2. Design of Consensus-Based Adaptive Controller

If power constraints are not considered, $L_i(P_i)$ could be identical by choosing the same $\lambda_i = \lambda_0$. However, the power of DERs is not limitless; P_i should keep the maximum or the minimum if DER i reaches its power limits. To finish this goal, we changed the cost coefficient, b_i , as listed in Equations (4) and (6), according to different conditions. Specifically, b_i is equal to $b_{i,\text{true}}$ (the true cost coefficient) if the power of DER i is between the minimum and the maximum. In contrast, if the power of DER i arrives at its upper or lower limit, b_i is equal to $b_{i,\text{virtual}}$ (the virtual cost coefficient), and $b_{i,\text{virtual}}$ should be adjusted to make DER i maintain the maximum or minimum power output. In other words, all DERs can be classified into two parts: restricted DERs (*maximum or minimum power output*) and unrestricted DERs (*output power between minimum and maximum*). The virtual cost coefficient, $b_{i,\text{virtual}}$, for restricted DERs should be regulated to make the true marginal costs for unrestricted DERs the same, and meanwhile, the power of restricted DERs keeps the maximum or the minimum. In this paper, on the basis of continuous-time consensus algorithms [25], we designed a consensus-based adaptive controller to adjust the virtual cost coefficient, $b_{i,\text{virtual}}$, of restricted DERs, which will be discussed in Sections 3.2.1 and 3.2.2.

Specially, for the storage devices, capacity constraints should also not be neglected. If the storage capacity has increased to 80% or decreased to 20% of its maximum capacity, its virtual cost coefficient, $b_{i,\text{virtual}}$, is adjusted, to draw the power of the storage to zero.

3.2.1. Conventional Generators and Renewable Generators (CG and RG)

The adaptive controller of CGs is listed as,

$$b_{i,virtual} = \frac{\int \sum_{j \in N_i} a_{ij} (\lambda_j L_j(P_j) - \lambda_i L_i(P_i))}{\lambda_i} - 2a_i P_{i,max} \quad P_i \geq P_{i,max} \quad (21a)$$

$$b_i = b_{i,true} \quad 0 \leq P_i < P_{i,max} \quad (21b)$$

$$b_{i,virtual} = \frac{\int \sum_{j \in N_i} a_{ij} (\lambda_j L_j(P_j) - \lambda_i L_i(P_i))}{\lambda_i} \quad P_i < 0 \quad (21c)$$

where $\mathbf{A} = [a_{ij}]_{n \times n}$ is the weighted adjacency matrix of communication topology with elements $a_{ij} = a_{ji} \geq 0$. This means that if node i can send/receive information to/from node j , $a_{ij} > 0$, otherwise, $a_{ij} = 0$. The set of neighbors for node i is denoted by $N_i = \{d_j \in d : (d_i, d_j) \in \chi\}$. For Equations (21a) and (21c), the true marginal cost $L_i(P_{i,max}/0, b_{i,true})$ is a constant for restricted CG i and $b_{i,virtual}$ will change with the regulating process with other DERs until $\lambda_i L_i(P_{i,max}/0, b_{i,virtual}) = \lambda_j L_j(P_j) = 1/n \sum_{k=1}^n \lambda_k L_k(P_k)$ for all $i, j \in (1, 2, \dots, n)$. In contrast, for Equation (21b), $L_i(P_i)$ will change according to the economic droop coefficient, $\lambda_i = \lambda_0$, until the system gradually becomes stable for unrestricted CGs. In detail, when the output power of one CG locates between minimum and maximum, the cost coefficient, b_i , is given, based on Equation (21b). If the output power has reached the upper or lower limits, Equation (21a) or (21c) is used to refresh the coefficient. It is worthwhile to mention that for Equations (21a) and (21c), only virtual marginal costs are regulated and true marginal costs have always been unchanged.

Similar to [25], when the system gradually becomes stable, the virtual cost coefficient for restricted DER i is determined by the weighted average of economic droop coefficients and marginal costs of its neighbors. The specific equation is presented as:

$$b_i = \begin{cases} b_{i,virtual} = \frac{\sum_{j \in N_i} w_{ij} \lambda_j L_j(P_j)}{\lambda_i} - 2a_i P_{i,max} & P_i \geq P_{i,max} \\ b_{i,virtual} = \frac{\sum_{j \in N_i} w_{ij} \lambda_j L_j(P_j)}{\lambda_i} & P_i < 0 \end{cases} \quad (22)$$

$$w_{ij} = \frac{a_{ij}}{\sum_{k \in N_i} a_{ik}}$$

Similarly, the adaptive controller of RGs can be presented as:

$$b_{i,virtual} = \frac{\int \sum_{j \in N_i} a_{ij} (\lambda_j L_j(P_j) - \lambda_i L_i(P_i))}{\lambda_i} - 2 \frac{1}{P_{i,max}} P_{i,max} \quad P_i \geq P_{i,max} \quad (23a)$$

$$b_i = b_{i,true} \quad 0 \leq P_i < P_{i,max} \quad (23b)$$

3.2.2. Storage Devices (Sd)

In contrast to CGs and RGs, the capacity limits of Equation (24) must be included into the adaptive controller for the storage devices. $W_i(0)$ is the initial capacity of the storage i , Δt indicates the system's operating time, and $W_i(\Delta t)$ indicates the remaining capacity after a period of time Δt . When the capacity, $W_i(\Delta t)$, of storage i is larger than 80% of the maximum capacity, $W_{i,max}$, or smaller than 20%

of $W_{i,\max}$, the virtual cost coefficient, $b_{i,\text{virtual}}$, should be adjusted to gradually make the power, P_i , of storage i zero. The adaptive controller of storage i is shown in Equation (25).

$$\begin{aligned} W_i(\Delta t) &= W_i(0) - P_i \Delta t \\ 0 &\leq W_i(\Delta t) \leq W_{i,\max} \end{aligned} \quad (24)$$

$$\begin{aligned} &\text{if } P_i \geq P_{i,\max} \text{ and } 20\%W_{i,\max} \leq W_i(\Delta t) \leq 80\%W_{i,\max} \\ b_{i,\text{virtual}} &= \frac{\int \sum_{j \in N_i} a_{ij} (\lambda_j L_j(P_j) - \lambda_i L_i(P_i))}{\lambda_i} - 2a_i P_{i,\max} \end{aligned} \quad (25a)$$

$$\begin{aligned} &\text{if } P_i \leq -P_{i,\max} \text{ and } 20\%W_{i,\max} \leq W_i(\Delta t) \leq 80\%W_{i,\max} \\ b_{i,\text{virtual}} &= \frac{\int \sum_{j \in N_i} a_{ij} (\lambda_j L_j(P_j) - \lambda_i L_i(P_i))}{\lambda_i} + 2a_i P_{i,\max} \end{aligned} \quad (25b)$$

$$\begin{aligned} &\text{if } -P_{i,\max} < P_i < P_{i,\max} \text{ and } 20\%W_{i,\max} \leq W_i(\Delta t) \leq 80\%W_{i,\max} \\ b_{i,\text{true}} & \end{aligned} \quad (25c)$$

$$\begin{aligned} &\text{if } W_i(\Delta t) \geq 80\%W_{i,\max} \text{ or } W_i(\Delta t) \leq 20\%W_{i,\max} \\ b_{i,\text{virtual}} &= \frac{\int \sum_{j \in N_i} a_{ij} (\lambda_j L_j(P_j) - \lambda_i L_i(P_i))}{\lambda_i} \end{aligned} \quad (25d)$$

4. Distributed Secondary Control

In this paper, DSFC was proposed to restore the network frequency; the DSVC based on [10] was used to coordinate the voltage regulation and reactive-power averaging, on the basis of the primary controller Equation (30). In this paper, we put more emphasis on voltage regulation.

4.1. Secondary Frequency Control

The DSFC are listed as:

$$f_i = f^* - \lambda_i L_i(P_i) + \Delta f_i \quad (26)$$

$$\Delta f_i = \frac{1}{k_i} \int_0^t \left[(f^* - f_i) + \sum_{j \in N_i} b_{ij} (\Delta f_j - \Delta f_i) \right] dt \quad (27)$$

where Δf_i is the secondary control variable, k_i is a positive gain that determines the speed of frequency regulation, and b_{ij} ($b_{ij} > 0$) is the corresponding weighted parameter of the $n \times n$ adjacency matrix \mathbf{B} of MGC communication topology, and b_{ij} is closely related with the accuracy of $L(P)$ -sharing. A large-signal nonlinear stability analysis of traditional droop control was introduced in [29], yielding the steady-state network frequency, f_{ss} ,

$$f_{ss} = f^* - P_0 / \sum_{i=1}^n \frac{1}{m_i} \quad (28)$$

where P_0 is the total active-power load in the network. Similarly, for Equation (29), the steady-state network frequency f_{ss1} can be obtained as:

$$\begin{aligned} f_{ss1} &= f^* - \sum_{i=1}^n L_i(P_i) / \sum_{i=1}^n \frac{1}{\lambda_i} \\ \sum_{i=1}^n P_i &= P_0 \end{aligned} \quad (29)$$

4.2. Secondary Voltage Control

The DSVLC are presented as:

$$E_i = E^* - n_i Q_i + \Delta E_i \quad n_i = \frac{E_{\max} - E_{\min}}{Q_{i,\max}} \tag{30}$$

$$\Delta E_i = \frac{1}{r_i} \int_0^t \left[\eta_i (E^* + \int_0^t (E^* - U_i) dt - E_i) + \sum_{j \in N_i} c_{ij} \left(\frac{Q_j}{Q_{j,\max}} - \frac{Q_i}{Q_{i,\max}} \right) \right] dt \tag{31}$$

where E_{\max}, E_{\min} are the upper and lower voltage limits, $Q_{i,\max}$ is the allowable reactive power maximum, E^* is the rated network voltage, Q_i is the measured reactive power injection, E_i is the referenced voltage magnitude, used to generate three-phase PWM (Pulse Width Modulation) impulses. The gain n_i is the relevant droop coefficient. ΔE_i is the secondary control variable, U_i is the measured output voltage magnitude at the load node of DER i , r_i, η_i are positive gains, that are respectively responsible for the speed and accuracy of voltage regulation, the $n \times n$ matrix C , with elements $c_{ij}(c_{ij} > 0)$, is the adjacency matrix of MGC communication topology, and c_{ij} is closely related to the accuracy for reactive power averaging. A small-signal stability analysis of Equation (31) can be found in [10,30]. Due to the previously proposed conflict between reactive power averaging and voltage regulation, the proper gains, η_i and c_{ij} , should be chosen to guarantee the stability of Equation (30). More discussion can be found in [10]. In this paper, the main goal was to regulate and restore the voltage magnitudes.

5. The Implementation of the Overall Distributed Economic Control

5.1. Communication Network Topology of MGC

The communication network topology of distributed economic control of MGC under study in this paper is shown in Figure 1, including the communication network inside sub-microgrids and between sub-microgrids. Each DER is configured with a distributed controller (DCr), which is responsible for communication and distributed strategy. In autonomous mode, each DCr exchanges with each other through the communication network inside sub-microgrids. In collective mode, one or two DCr inside sub-microgrids are chosen to communicate with their neighbor’s sub-microgrids, and so the communication link between sub-microgrids is built. The proposed strategy makes use of original distributed controller of each DER, and combines the control of single microgrids and the control of MGC. In addition, it is unnecessary to configure the controller for MGC, and therefore lower the installation costs.

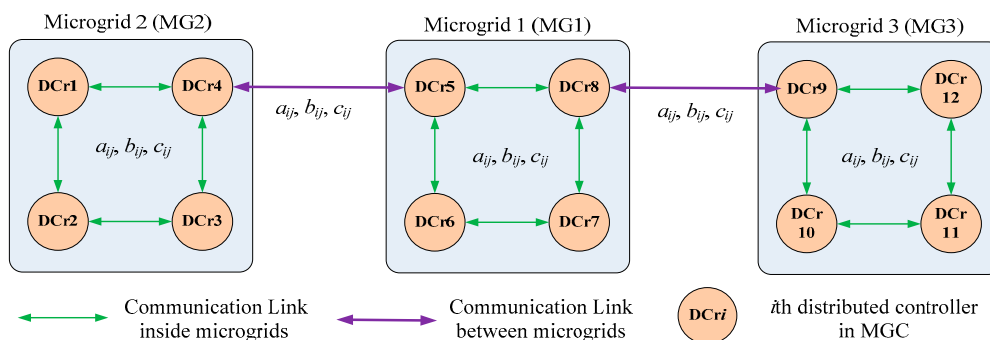


Figure 1. Communication network topology of the microgrid cluster (MGC) under study.

Moreover, the calculation of LLCF needs to obtain the voltage magnitudes of the connected nodes in the electric circuit, so the interconnected nodes in electric circuit need to be equipped with communication links, and for unconnected nodes, it is optional whether to communicate according

to optimization network topology. It is worthwhile to mention that a_{ij} , b_{ij} , c_{ij} varies with different consensus network topology, in different operating modes.

5.2. Overall Control Architecture

A detailed graph of the overall control architecture for a single DER, applying primary economic droop controller Equation (19), adaptive controller Equation (21) for CGs, Equation (23) for RGs, Equation (25) for the storage, primary voltage droop controller Equation (30), DSFC Equation (27) and DSVC Equation (31), is shown in Figure 2.

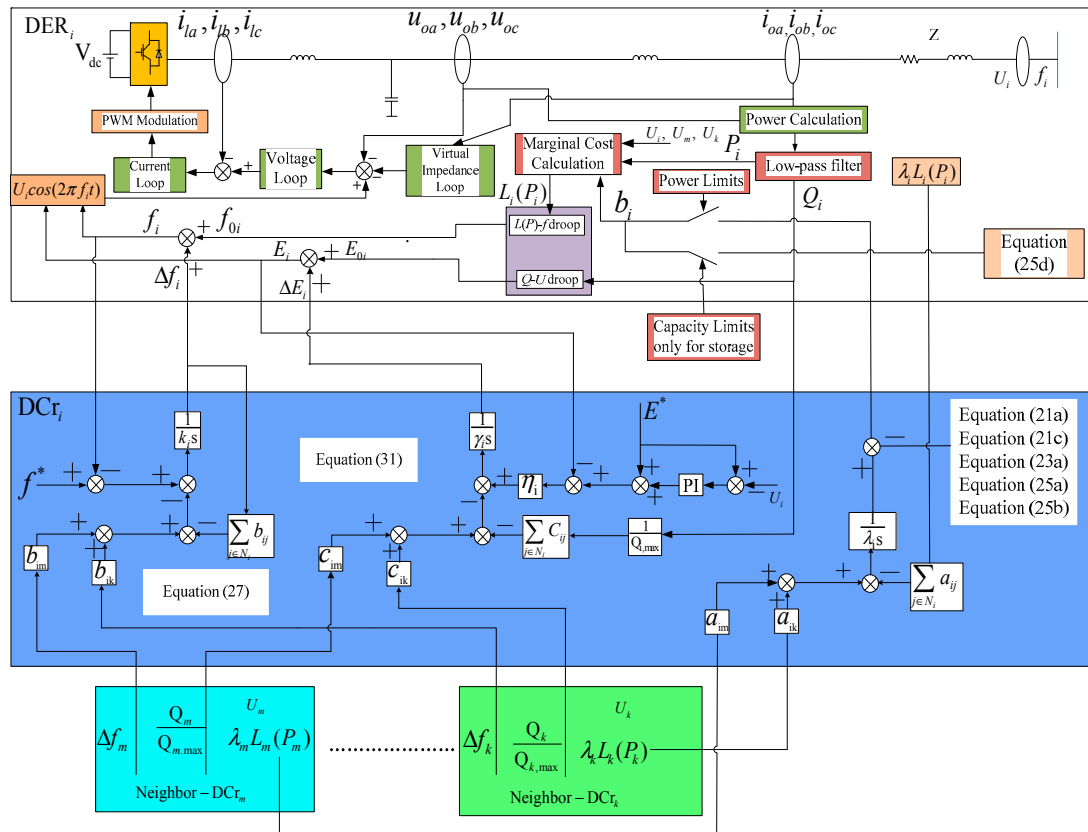


Figure 2. Block diagram of the overall control architecture for a single distributed energy resource (DER).

In a distributed sparse communication network, each DCr only interacts with information from adjacent DCrs, so high reliability can be achieved, as a dominant DCr is not necessary. Taking DER i for an example, DCr i sends its relevant information ($Q_i, \Delta f_i, \lambda_i L_i(P_i), U_i$) to its neighbor's DCr j as well as receiving the relevant information ($Q_j, \Delta f_j, \lambda_j L_j(P_j), U_j$) from adjacent DCr j , and then the distributed strategy is applied to complete the goal of frequency recovery, voltage regulation, and the regulation of the cost coefficient, b_i , when the power bounds or capacity constraints, only for the storage, arrive.

The proposed distributed strategy can successfully realize the transition between autonomous mode and collective mode, as listed in Equation (18). Autonomously, the power is distributed by identical TMC inside sub-microgrids; Collectively, the generation costs of the whole MGC can be effectively lowered by considering line loss to realize LLMC same. Moreover, the system frequency can be restored to the rating, and node voltage magnitudes can be regulated near to the nominal value.

6. Simulation Results

This section presents simulation results to validate the effectiveness of the proposed controllers. A MGC, incorporating three sub-microgrids, as shown in Figure 3, was used to test the distributed economic strategy under a series of scenarios, and the topology of the communication network is presented in Figure 1, with adjacency matrices $\mathbf{A} = [a_{ij}]$, $\mathbf{B} = [b_{ij}]$ and $\mathbf{C} = [c_{ij}]$ being respectively listed in Equation (32). The impedances ($Z1, Z2, Z3$) of three sub-microgrids were, respectively, $0.2 + j0.012 \Omega$, $0.3 + j0.018 \Omega$, $0.4 + j0.027 \Omega$; the impedances of $Z4, Z5, Z6$ and $Z7$ were all $0.1 + j0.006 \Omega$. In addition, the impedance between the other sub-microgrids were as follows: $ZM12 = 0.8 + j0.056 \Omega$, $ZM13 = 0.9 + j0.062 \Omega$. For all DERs, $\lambda_i = \lambda_0 = 0.001$, $k_i = 0.02$, $r_i = 0.01$, $\eta_i = 5$, $n_i = 1 \times 10^{-4}$ and $Q_{i,max} = 20$ kVAR. The simulation was built in Matlab/Simulink, and other important simulation parameters are listed in Table 1.

$$\mathbf{A} = \left[a_{ij} = \begin{cases} 0 & \text{others} \\ 1 & j \in N_i \end{cases} \right], \mathbf{B} = \left[b_{ij} = \begin{cases} 0 & \text{others} \\ 1.5 & j \in N_i \end{cases} \right], \mathbf{C} = \left[c_{ij} = \begin{cases} 0 & \text{others} \\ 20 & j \in N_i \end{cases} \right] \quad (32)$$

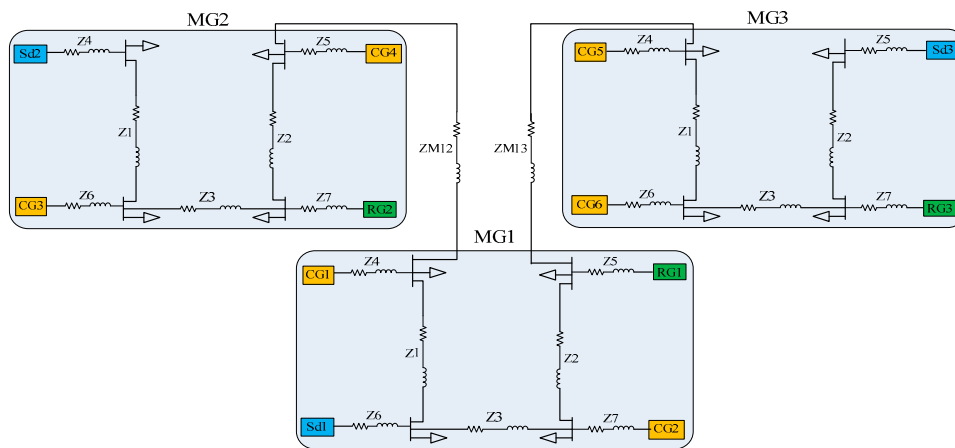


Figure 3. Schematic of the MGC under study, incorporating three sub-microgrids.

Table 1. Simulation parameters.

	$a_i / [\text{€} \cdot (\text{kW} \cdot \text{W} \cdot \text{h})^{-1}]$	$b_{i,true} / [\text{€} \cdot (\text{kW} \cdot \text{h})^{-1}]$	$P_{i,max}$
CG1/CG2	0.0034/0.0076	5.6/2.6	20 kW/18 kW
CG3/CG4	0.0063/0.0031	3.5/4.7	15 kW/16 kW
CG5/CG6	0.0034/0.0016	3.5/4.9	18 kW/20 kW
RG1/RG2/RG3	$1.43 \times 10^{-4} / 2 \times 10^{-4} / 1.67 \times 10^{-4}$	-2	7 kW/5 kW/6 kW
Sd1/Sd2/Sd3	$\frac{a_k}{0.00008/0.00005/0.00004}$ $\frac{\bar{a}_k}{0.015/0.010/0.005}$	0	8 kW/10 kW/14 kW

6.1. Case 1: Performance Analysis and Cost Comparison

In Case 1, the operating performance in MGC is shown in Figure 4. Before 5 s, each MG (MG1, MG2, MG3) operates autonomously and the active power of all DERs is distributed by TMC. Thus, apart from marginal costs of RGs, the marginal costs between MGs are not identical; however, the marginal costs inside MGs are the same—that is, each MG economically operates in autonomous mode. Between 5 s and 10 s, all MGs are integrated into MGC and LLMC is used to distribute power for each DER. Eventually marginal costs are the same for all MGs, except from those of RGs and CG6, which have already reached their upper limits, and the MGC is operated by the optimum state. After 10 s, CG4 has also arrived at its maximum output, through the combined effects of cheaper prices and heightened loads, and so the marginal costs of both CG4 and CG6 do not change anymore. Therefore, an identical LLMC is achieved among other DERs. Later, the LLMC is adjusted to jointly stabilize at

a lower level for all DERs, except RGs, due to a greatly decreased load demand after 15 s. From the view of maximum utilization of renewable energy, RGs always keep the maximum output in the whole operating process—respectively 7 kW, 5 kW and 6 kW—thus their marginal costs are all zero all the way. As shown in Figure 4c,d, the system frequency can always stay stable at the nominal value, $f^* = 50$ Hz, regardless of some small fluctuations. The voltage magnitudes of all DERs can be adjusted to around the rated value, $E^* = 311$ V, with a largest error of 3 V, yet the error is permitted, due to heterogeneous impedances in the network. Due to the main goal of voltage regulation, the reactive power is not shared by the capacity ratio of all DERs.

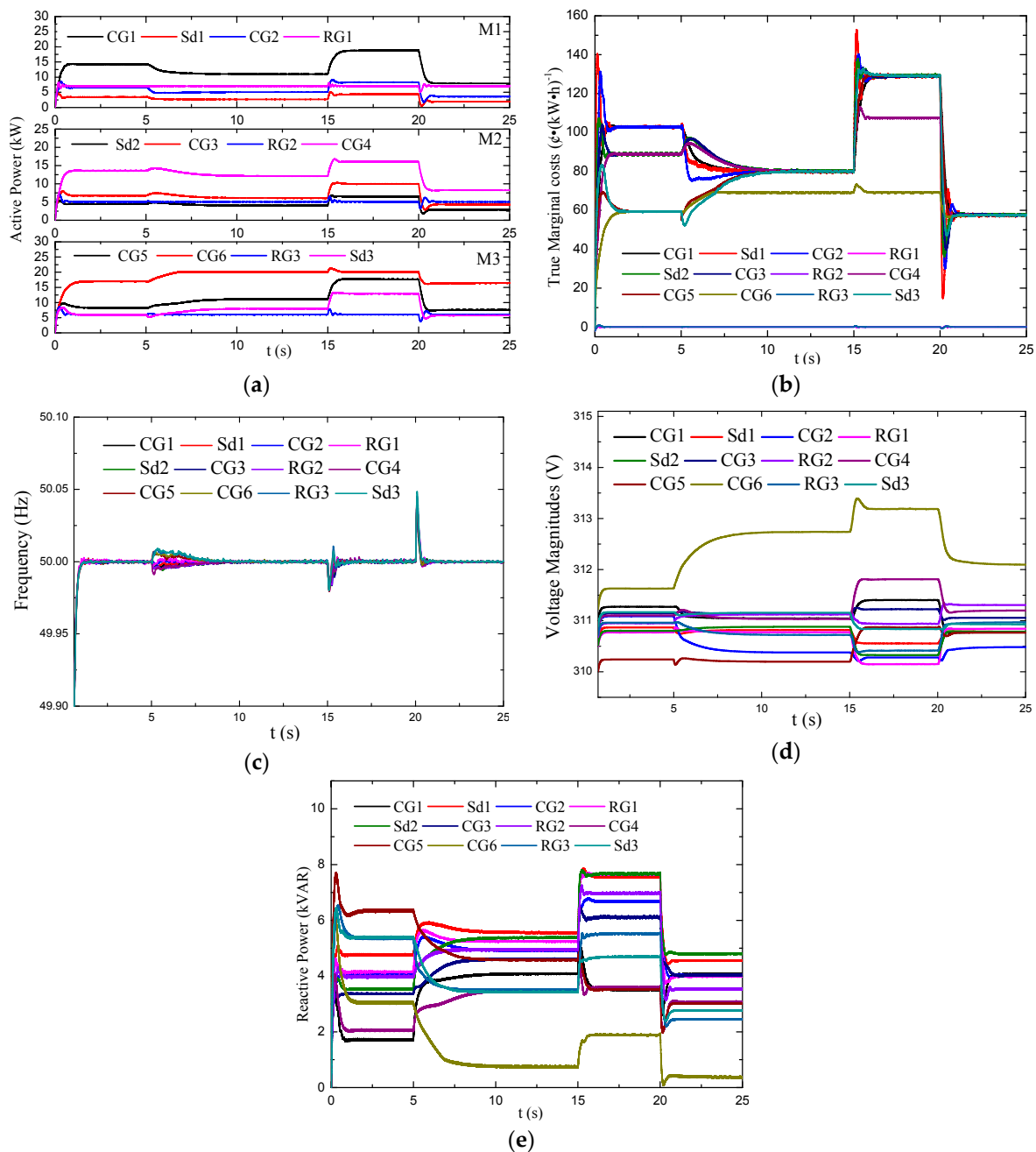


Figure 4. The operating performance in MGC: (a) Active power outputs of DERs; (b) The true marginal costs of DERs; (c) The system frequency; (d) The voltage magnitudes; (e) Reactive power outputs of DERs.

Figure 5 gives the active power obtained by traditional droop control in MGC, where the operating conditions are the same with Figure 4. From Figure 5, the power of all DERs are generated by the capacity ratio. Specially, after 5 s, when M1, M2 and M3 are integrated into MGC, CG1 and CG6, they generate the same power, due to having the same capacity (20 kW), and the power is also identical for CG2 and CG5 with the same capacity (18 kW). For RGs, in comparison with Figure 4a, where the maximum power is always generated to maximize the utilization of renewable energy, the power has not arrived at the maximum, all the way, for the traditional droop control—this will largely increase the system expenses. The specific total generating costs comparison for the traditional droop control and the proposed economy method are shown in Table 2. From Table 2, the total costs of MGC are always lower when using the proposed method, compared to that of the traditional droop control, in every time step, and cost reduction can be up to 34.99%. The main reasons for cost reduction are that more power is generated by cheap DERs and the maximum usage of RGs. Moreover, the capacity of expensive DERs is higher and the cost reduction is larger.

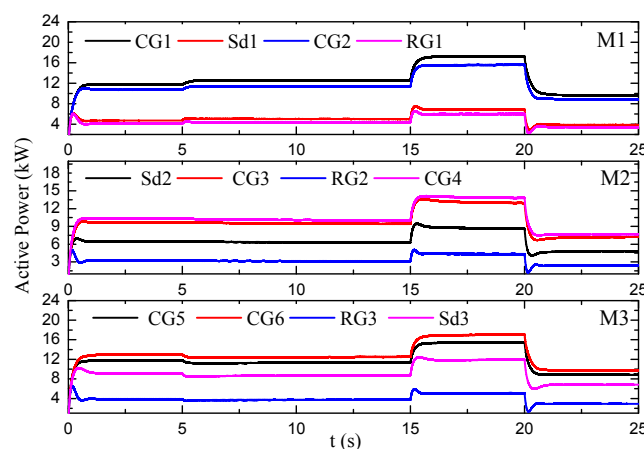


Figure 5. The active power using the traditional droop control in MGC.

Table 2. Comparison of total generating costs, using different methods in MGC.

Time/s	Total Generating Costs of MGC/[$\$/(\text{h})^{-1}$]		Costs Reduction/%
	Traditional Droop	Proposed Method	
0~5	45.23	34.30	24.16
5~15	44.51	32.42	27.16
15~20	83.55	67.69	18.98
20~25	27.43	17.83	34.99

6.2. Case 2: Considering the Varying Maximum Power of RGs

Because the predicted maximum power of RGs often varies in actual conditions, Figure 6 shows the operating characteristics of MGC, considering varying maximum powers of RGs. The sum of loads is unchanged in the whole process, and the predicted maximum power of RG3 is also fixed at 6 kW all the time. In contrast, the predicted maximum power of RG1 decreases from 7 kW to 4 kW, by 1 kW, for each 5 s, and on the contrary, the predicted maximum power of RG2 increases from 5 kW to 8 kW, by 1 kW, for each 5 s. As shown in Figure 6, as predicted, the power of RGs always arrives at the predicted maximum power for economy maximization, specifically, 7 kW to 6 kW to 5 kW to 4 kW for RG1, 5 kW to 6 kW to 7 kW to 8 kW for RG2, and always 6 kW for RG3. Thus, the marginal costs of RGs are zero all the time, as computed in Equation (4). It can be also clearly seen that, apart from RGs, the power of other DERs stays unchanged all the way, due to fixed loads and a fixed sum of the power of RGs. Thereinto, the upper power limits of CG6 are reached, because of cheaper price, and thus its

marginal costs are always lower than those of other DERs. Apart from RGs and CG6, the marginal costs of other DERs are the same to realize economic operation and unchanged due to fixed power output the whole time.

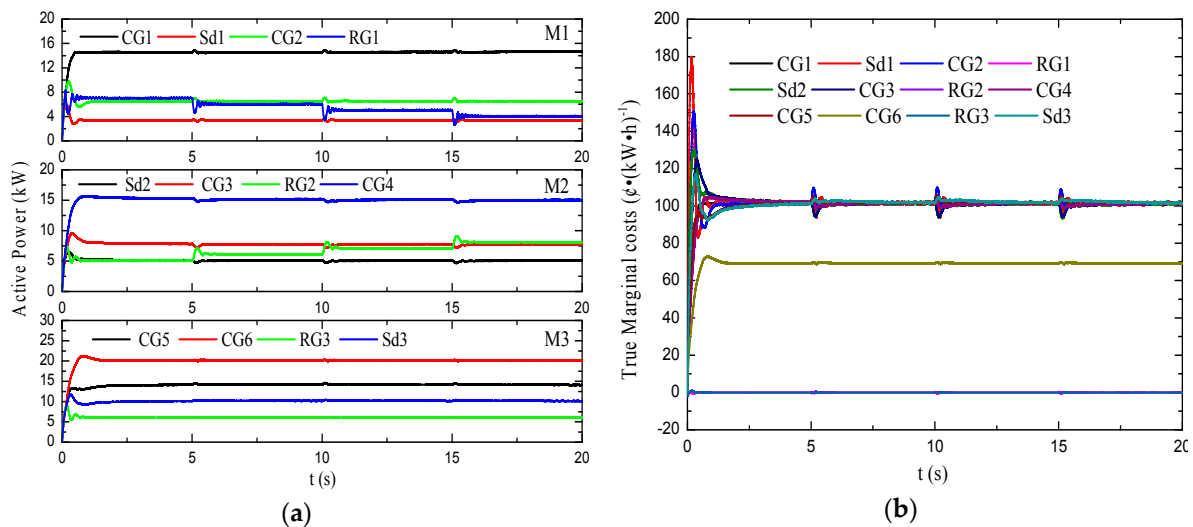


Figure 6. The operating characteristics with varying maximum powers of RGs: (a) Active power outputs of DERs; (b) The true marginal costs of DERs.

6.3. Case 3: The Optimization of Storage Devices

Figure 7 gives the active power and marginal cost of each DER, considering storage (Sd2) optimization; we assume the initial capacity and maximum capacity of Sd2 are, respectively, 12 kW·s and 30 kW·s. The capacity of Sd2 with the operating time is drawn in Figure 8. Before 10 s, the MGC is operating in a light load scenario, conventional generators CG1~CG6 do not generate any active power due to expensive expenses, and their marginal costs maintain different constants. According to Equations (4)–(6), the storages, Sd1, Sd2 and Sd3, are charged and the active power of RGs is generated to simultaneously satisfy the load demand and charging demand of the storages, and their power is proportional to their predicted power capacity, as mentioned in Equation (7). At about 6 s, the capacity of Sd2 has arrived at 80% of the maximum, thus Equation (25d) starts to make the charging power of Sd2 equal to zero. Meanwhile, the power of RGs is reduced, but still proportional, and the charging power of Sd1/Sd3 is raised, to maintain the power balance. Later, the capacity of Sd2 stays nearly unchanged. Before applying Equation (25d), the marginal costs of RGs and Sds stay identical and the marginal cost of Sd2 becomes zero and is no longer the same with those of others, due to the application of Equation (25d) after about 6 s. After 10 s, the load demand increases a lot, the power of RGs keeps their maximum output in the view of maximum exploitation of renewable energy, and so the marginal costs of RGs are zero all the way. For CGs, their power dramatically increases, to satisfy load demands. In particular, Sds change their operating states from charging to discharging. At around 16 s, the capacity of Sd2 lowers to 20% of the maximum capacity, Equation (25d) is applied again to decrease the discharging power of Sd2 equal to zero, and thus the capacity of Sd2 hardly changes anymore. Between 10 s and 14 s, the marginal costs of CGs and Sds are the same, to achieve the economic operation of MGC, and after 14 s, Sd2 largely reduces its marginal costs to zero; the marginal costs of CGs and other Sds arrive at a higher level to compensate for the power reduction of Sd2.

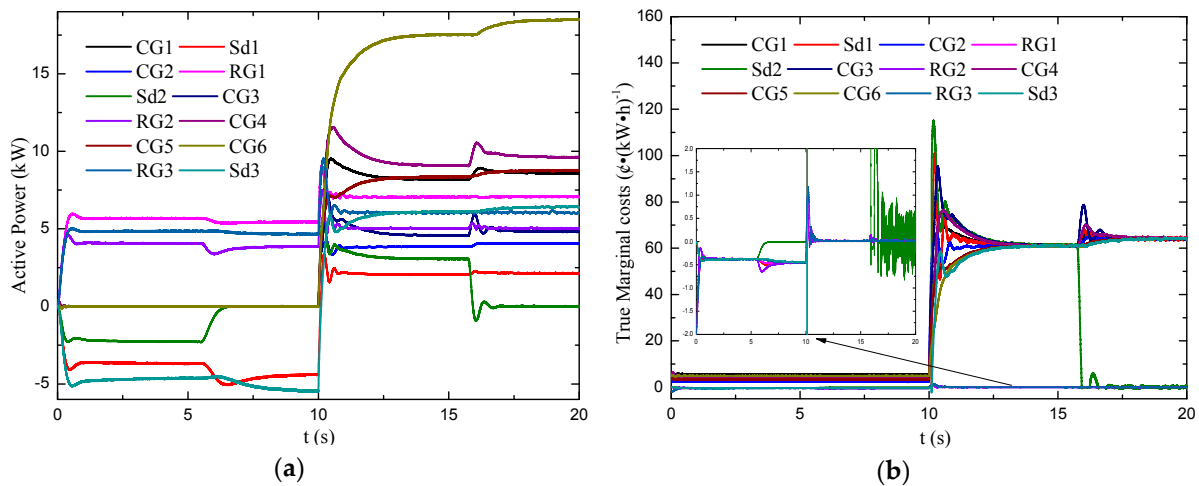


Figure 7. The results, considering storage device (Sd2) optimization: (a) Active power outputs of DERs; (b) The true marginal costs of DERs.

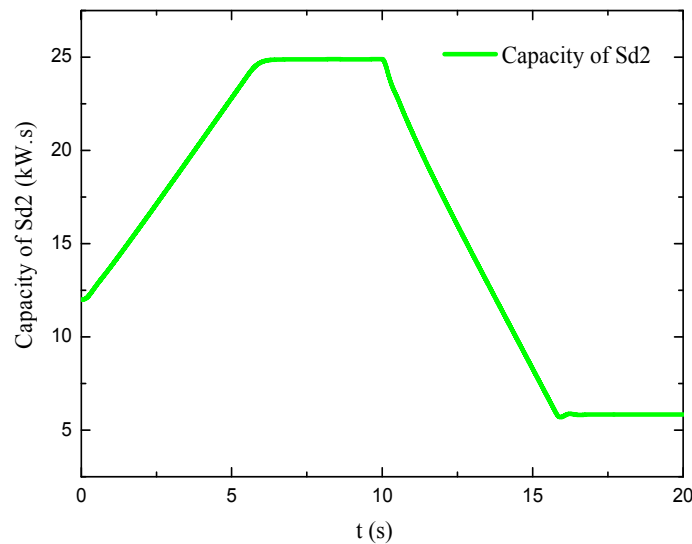


Figure 8. The capacity of Sd2.

6.4. Case 4: The Effect of Communication Delays

Figure 9 gives the regulating process of frequency restoration, considering different communication delays, respectively, 0 ms, 1 ms, 3 ms, 5 ms and 10 ms. In this paper, only the communication delays among sub-microgrids are considered and we can see that the overshoot tends to enlarge with increasing communication delays; that is, the communication delays can affect the transient performance of the whole design. However, the time of coming to the steady state is nearly unchanged. On the other hand, the proposed strategy is still effective for relatively longer delays (10 ms); thus, it can be deduced that the design is robust and available in actual conditions.

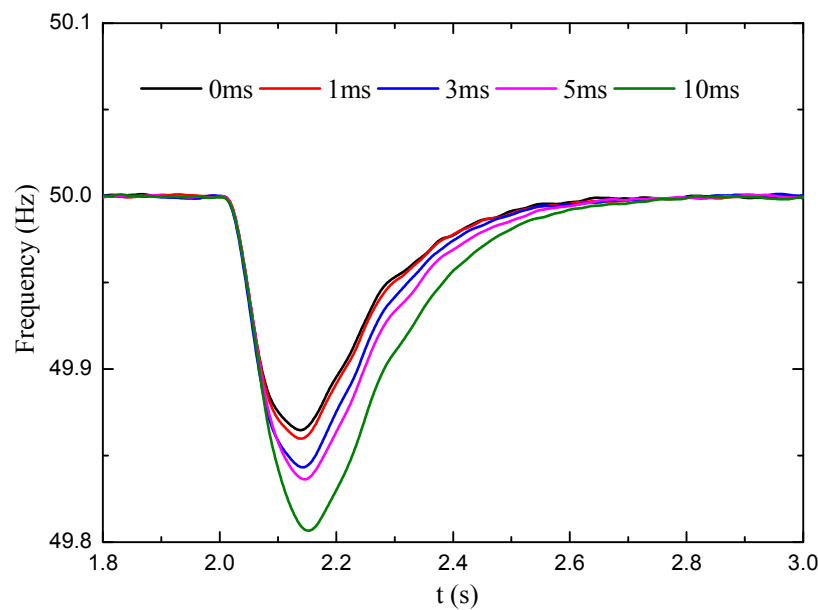


Figure 9. The comparison of frequency regulation with different communication delays.

7. Conclusions

Aimed at the higher operating expenses of MGC brought by the traditional droop control, this paper proposed a distributed economic strategy to lower the whole operating costs. A consensus-based adaptive controller was proposed, to deal with power limits of DERs. In particular, for storage devices, capacity constraints were also included. The renewable generators were modeled to minimize the curtailment, and the storage was modeled to charge or discharge, according to different load conditions. Moreover, the distributed secondary control was used to restore the system frequency and voltage magnitudes of DERs. In addition, the whole design was able to achieve the transition between autonomous mode and collective mode, and line loss was considered, to further lower the expenses in collective mode. More importantly, the proposed strategy does not need the central controller, and has a high reliability, only using sparse communication network among neighbors.

However, the communication delay can affect the transient performance of the whole design (i.e., overshoot); therefore, determining how to lower the effect of communication delays is necessary in the future.

Acknowledgments: The authors gratefully acknowledge the support of the National Major Research and Development Program of China (2016YFB0901302), and the support of National Natural Science Foundation of China (51577115).

Author Contributions: All the authors contributed to this work. Xiaoqian Zhou designed the study, performed the analysis, performed simulations, and wrote the first draft of the paper. Qian Ai set the simulation environment and checked the overall logic of this work. Hao Wang contributed to provide important comments on the modeling and thoroughly revised the paper.

Conflicts of Interest: The authors declare no conflict of interest.

References

1. Yang, X.; Su, J.; Lü, Z. Overview on micro-grid technology. *Proc. CSEE* **2014**, *34*, 57–70.
2. Hernandez, C.L.; Mirez, T.J.; Horn, M.; Bonilla, L. Simulation of direct current microgrid and study of power and battery charge/discharge management. *DYNA* **2017**, *92*, 673–679.
3. Ganesan, S.; Padmanaban, S.; Varadarajan, R. Study and analysis of an intelligent microgrid energy management solution with distributed energy sources. *Energies* **2017**, *10*, 1419. [[CrossRef](#)]
4. Zhi, N.; Xiao, X.; Tian, P.G. Research and prospect of multi-microgrid control strategies. *Electr. Power Autom. Equip.* **2016**, *36*, 107–115.

5. Moayedi, S.; Davoudi, A. Distributed tertiary control of DC microgrid clusters. *IEEE Trans. Power Electron.* **2015**, *31*, 1717–1733. [[CrossRef](#)]
6. Shafiee, Q.; Dragicevic, T.; Andrade, F. Distributed consensus-based control of multiple DC-microgrids clusters. In Proceedings of the IEEE Industrial Electronics Society (IECON 2014), Dallas, TX, USA, 29 October–1 November 2014; IEEE: New York, NY, USA, 2014; pp. 2056–2062.
7. Adhikari, S.; Qianwen, X.U.; Tang, Y. Decentralized control of two DC microgrids interconnected with tie-line. *J. Mod. Power Syst. Clean Energy* **2017**, *5*, 599–608. [[CrossRef](#)]
8. Mohamed, A.A.; Elsayed, A.T.; Youssef, T.A. Hierarchical control for DC microgrid clusters with high penetration of distributed energy resources. *Electr. Power Syst. Res.* **2017**, *25*, 140–148. [[CrossRef](#)]
9. Zhou, X.; Chen, Y.; Zhou, L. A microgrid cluster structure and its autonomous coordination control strategy. *Trans. China Electrotechnol. Soc.* **2017**, *32*, 123–134.
10. Simpson-Porco, J.W.; Shafiee, Q.; Dörfler, F. Secondary frequency and voltage control of islanded microgrids via distributed averaging. *IEEE Trans. Ind. Electron.* **2015**, *62*, 7025–7038. [[CrossRef](#)]
11. Real, A.J.D.; Arce, A.; Bordons, C. Combined environmental and economic dispatch of smart grids using distributed model predictive control. *Int. J. Electr. Power Energy Syst.* **2014**, *54*, 65–76. [[CrossRef](#)]
12. Yang, J. Consensus algorithm based real-time collaborative power dispatch for island multi-microgrid. *Autom. Electr. Power Syst.* **2017**, *41*, 8–15.
13. David, G.; Javier, M. Distributed energy trading: The multiple-microgrid case. *IEEE Trans. Ind. Electron.* **2015**, *62*, 2551–2559.
14. Mohammad, F.; Hassan, B. Statistical cooperative power dispatching in interconnected microgrids. *IEEE Trans. Sustain. Energy* **2013**, *4*, 586–593.
15. Guo, F.; Wen, C.; Mao, J. Distributed economic dispatch for smart grids with random wind power. *IEEE Trans. Smart Grid* **2016**, *7*, 1572–1583. [[CrossRef](#)]
16. Yu, Z.; Ai, Q.; Gong, J. A novel secondary control for microgrid based on synergetic control of multi-agent system. *Energies* **2016**, *9*, 243. [[CrossRef](#)]
17. Yu, Z.; Ai, Q.; He, X. Adaptive droop control for microgrids based on the synergetic control of multi-agent systems. *Energies* **2016**, *9*, 1057. [[CrossRef](#)]
18. Lin, Y.L.; Chia, C.C. Consensus-based secondary frequency and voltage droop control of virtual synchronous generators for isolated AC micro-grids. *IEEE J. Emerg. Sel. Top. Circuits Syst.* **2015**, *5*, 443–455.
19. Fang, H.; Chang, Y.W.; Jian, F.M.; Yong, D.S. Distributed secondary voltage and frequency restoration control of droop-controlled inverter-based microgrids. *IEEE Tran. Ind. Electron.* **2015**, *62*, 4355–4364.
20. Nutkani, I.U.; Loh, P.C.; Blaabjerg, F. Droop scheme with consideration of operating costs. *IEEE Trans. Power Electron.* **2013**, *29*, 1047–1052. [[CrossRef](#)]
21. Nutkani, I.U.; Loh, P.C.; Wang, P. Autonomous droop scheme with reduced generation cost. *IEEE Trans. Ind. Electron.* **2014**, *61*, 6803–6811. [[CrossRef](#)]
22. Nutkani, I.U.; Loh, P.C.; Blaabjerg, F. Cost-based droop scheme with lower generation costs for microgrids. *IET Power Electron.* **2014**, *7*, 1171–1180. [[CrossRef](#)]
23. Chen, S.U.; Zajun, W.U.; Zhen, Y.L. Droop control based on marginal cost for distributed economic operation of islanded microgrid. *Electr. Power Autom. Equip.* **2016**, *36*, 59–66.
24. Xin, H.; Zhang, L.; Wang, Z. Control of island AC microgrids using a fully distributed approach. *IEEE Trans. Smart Grid* **2015**, *6*, 943–945. [[CrossRef](#)]
25. Zhang, Z.; Ying, X.; Chow, M.Y. Decentralizing the economic dispatch problem using a two-level incremental cost consensus algorithm in a smart grid environment. In Proceedings of the North American Power Symposium, Boston, MA, USA, 4–6 August 2011; IEEE: New York, NY, USA, 2011; pp. 1–7.
26. Zhong, Q.C.; Hornik, T. *Control of Power Inverters in Renewable Energy and Smart Grid Integration*; Wiley-IEEE Press: Hoboken, NJ, USA, 2013.
27. Guerrero, J.M.; Vicuna, L.G.D.; Matas, J. Output impedance design of parallel-connected UPS inverters with wireless load-sharing control. *IEEE Trans. Ind. Electron.* **2005**, *52*, 1126–1135. [[CrossRef](#)]
28. Wang, Z.; Wu, W.; Zhang, B. A fully distributed power dispatch method for fast frequency recovery and minimal generation cost in autonomous microgrids. *IEEE Trans. Smart Grid* **2015**, *7*, 19–31. [[CrossRef](#)]

29. Shafiee, Q.; Guerrero, J.M.; Vasquez, J.C. Distributed secondary control for islanded microgrids—A Novel Approach. *IEEE Trans. Power Electron.* **2013**, *29*, 1018–1031. [[CrossRef](#)]
30. Schiffer, J.; Seel, T.; Raisch, J. A consensus-based distributed voltage control for reactive power sharing in microgrids. In Proceedings of the Control Conference, Strasbourg, France, 24–27 June 2014; IEEE: New York, NY, USA, 2014; pp. 1299–1305.



© 2017 by the authors. Licensee MDPI, Basel, Switzerland. This article is an open access article distributed under the terms and conditions of the Creative Commons Attribution (CC BY) license (<http://creativecommons.org/licenses/by/4.0/>).